Design methodology of a two-degrees-of-freedom gravitational energy harvester

Design methodology of a two-degrees-of-freedom gravitational energy harvester

Design methodology of a two-degrees-of-freedom gravitational energy harvester

M Lo Monaco[a] and C Russo[a]

[a] Politecnico di Torino - Department of Mechanical and Aerospace Engineering, C.so Duca degli Abruzzi, Torino,10129, Italy

E-mail: mirco.lomonaco@polito.it

Abstract. The growing spread of IoT (Internet of Things) and monitoring system based on micro electro-mechanical system (MEMS) concerns also the railway systems. The recent developments have made it possible to study and realize innovative integrated systems using connected devices. The technologies allow to collect real-time data from assets, thus providing fundamental information regarding the operation conditions and offering an evaluation of safety and durability of the monitored device. The major innovation of these devices is the use of energy harvesters to support or replace their power supply, making the monitoring device completely autonomous and drastically lowering the maintenance costs. The work presented in this paper is the product of the research group knowledge in vibrational energy harvesting. In particular, we studied a two-degrees-of-freedom (2DOF) gravitational vibration-based energy harvester (GVEH), characterized by the absence of the magnet on the top end of the tube, exploiting gravity as a restoring force. Different masses configuration were tested in order to find the best configuration optimizing power output, frequency bandwidth and overall performances. The time-domain simulations realized in Matlab/Simulink environment are supported with Multiboduy simulations for a better understanding of the system dynamics.

Keywords: energy harvesting, vibrations, electro-mechanical modeling, Autonomous Internet of Things

1. Introduction

The IoT devices and miniaturized monitoring systems has reached also the railway systems. Through these connected devices it is possible to have real-time information and data regarding the monitored vehicle or component. These new data offer the opportunity to have a new vision regarding the status of the monitored device, providing information now accessible thanks to the rising of these technologies. These devices and data provide the basis for the algorithms used to create Predictive Maintenance and Digital Twins, two tools that are acquiring visibility due to their key-role in the optimization of maintenance and safety procedures. The availability of a continuous stream of data allows to have knowledge on the health of the monitored system that can be crucial for the maintenance, safety, and design field [1],[2],[3]. Wireless monitoring networks are the tools for the continuous stream of data but must comply with some strict characteristics to be effective. These systems should have low power consumption, small size, long life cycles, and reliable wireless connections. It is necessary for the device to be small scaled for safe installations in hazardous or difficult-to-reach locations and to avoid interference with

the monitored system normal operations. Furthermore, for the purpose of having a reliable network and an affordable set of data, a strong wireless connection to the server and between the network nodes is essential. Finally, a long lifespan is necessary to lower the price of battery replacement and maintenance, following the low energy requirements. The batteries used in these networks are not sustainable in terms of cost, environmental disposal and safety. The major drawback of these systems, which should be created using the "install and forget" design principle, is the necessity of finding a reliable power supply in replacement of batteries. The absence of onboard power in freight vehicles enhances the design difficulties of these monitoring systems. Finding a solution to this issue is raising research interest in sustainable power supply options.

In literature, there are many research works regarding the design and study of energy harvesting devices in the railway field. The authors started their research with the study of one-degree-of-freedom (1DOF) vibrational energy harvester in the last decade [4]. The continuation of this work has led to recent publications [5],[6] and they are now proposing the design of two-degrees-of-freedom (2DOF) energy harvesters. These devices are studied in literature both with traditional and magnetic springs. The main advantage of 2DOF systems is the wider frequency bandwidth at high power with respect to a 1DOF system. Furthermore, the velocity amplification of the top magnet due to momentum transfer, results in higher output power. The mass ratio of the two moving magnets is a relevant design variable for these systems. Researchers have come to the conclusion that higher DOFs configurations are capable of harvesting energy over a wider frequency range, accepting lower maximum output [7]. These higher DOFs systems may be valid in applications with vibrational energy distributed over a wider frequency band, supplying devices with low power requirements. From the same research group of O'Donoghue, the work of Rodriguez et al. [8] is proposed, presenting a 2DOF velocity-amplified EM-VEH device. The novelty of this work is the possibility of varying the length of the tube, making the energy harvester frequencies tunable with the application. Always using a magnetic spring, in the work of Fan K. et al, [9] they deal with the generation of electricity exploiting ultra-low frequency excitations from human motion. This study introduces a 2DOF electromagnetic energy harvester (EMEH) as a solution to this issue. It is realized by the motion of a magnetically levitated 1DOF EMEH inside a cylindrical enclosure. The benefits of the suggested design, such as the tunable operating frequencies, increased power output, and expanded working bandwidth, are demonstrated both by experiments and modeling. The experimental results show that the proposed harvester achieves a rough 40 % improvement in power magnitude and a 152 % increase in operational bandwidth under a sinusoidal stimulation with an amplitude of 0.5 g. In railway field Chandarin U. et al [10] studies show the design and construction of a 2DOF vibration energy harvester for kinetic energy conversion via electromagnetic transduction. To successfully capture energy at two different frequencies, a coil is suspended as a second oscillating mass. The protoype resonance frequencies are set to coincide with the host structure prominent frequencies (i.e. heavy haul railcars). Peak output powers of 212 mW and 218 mW were produced via sinusoidal vibration at frequencies of 6.5 Hz and 14.5 Hz, respectively, with a peak acceleration of 0.4 g. A work from Feng Z. et al. [11] proposed a non-magnetic spring 2DOF energy harevster, using a serpentine planar spring. Compared with the conventional dual resonance harvester, the proposed system realizes an enhanced "band-pass" harvesting characteristic by increasing the relative displacement between magnet and coil among two resonance frequencies, pursuing a significant improvement in the average harvested power. The device produces an output power of 11 mW at the first resonant frequency of 58 Hz, 14.9 mW at the second resonant frequency of 74.5 Hz, and 0.52 mW at 65 Hz, which is in the middle of the two resonance frequencies. The frequency range of output power above 0.5 mW is from 55.8 Hz to 79.1 Hz.

This paper describes the design phases of a 2DOF vibrational energy harvester. Firstly, the structure of the energy harvester is described justifying the choice of the two masses. Secondly,

the analytical and numerical models in Matlab/Simulink environment are proposed with the support of the Ansys Maxwell FEM and Simpack Multibody simulations. The last section reports the model results and the conclusions.

2. Materials and methods

The devices analyzed in this work are cylindrical two-degrees-of-freedom gravitational vibrational energy harvesters (2DOF GVEHs). The purpose of these systems is to supply wireless sensor nodes along with a back-up rechargeable battery for condition-based monitoring of un-electrified freight wagons. The excitation frequencies on the coach coming from wheel-railroad contact are usually low due to suspensions filtering [4], depending on the type of boogie, train speed, railroad conditions and carried weight. GVEHs are well-suited for this application since the use of magnetic suspension results in a non-linear spring having low resonance frequency (1-50 Hz, [12]). Moreover, magnetic suspensions are low-cost and simple designs that can provide stable and long-lasting performances [13]. The main challenges of designing GVEHs for vehicle applications are finding the right trade-off between small device dimensions and low resonance frequency and tuning the resonant frequency with the fundamental frequency of the application. As mentioned before, for rail-freight cars it is necessary to design an energy harvester with a large bandwidth frequency in order to obtain power both in the tare and load condition.

2.1. Harvester configuration

The main components of a 2DOF GVEH include two suspended moving magnets, a fixed magnet at the bottom and coils wrapped around a tube. The moving magnets generate variable magnetic fluxes, inducing an alternating current in the coils, and return to their equilibrium positions under gravitational force. Maximum power is generated when the external excitation is in resonance with the masses of harvester. Consequently, the dimensioning of these generators is strictly dependent of their applications. Using a non-linear stiffness broadens the frequency range around the resonance frequency, thus increasing the system efficiency. The purpose of introducing a second degree of freedom with an additional non-linear stiffness is to further increase the high-power frequency range and overall efficiency. The 2DOF GVEH has a configuration that resembles a dynamic vibration absorber. Figure 1 reports a schematic representation of the system, along with further details on the components and their main dimensions. A radial clearance between the moving magnets and internal tube diameter is necessary to allow the longitudinal oscillation. However, undesired transversal motions arise that can be reduced by adding and internal guide for the moving magnets, preventing the performances decrease. The device has several coils made of enameled copper wires with same dimensions, number of turns, wire diameter and resistance. They are placed along the tube at different heights to find the axial location of the coil that optimizes the generated power. This phenomenon is linked to the variation of the magnetic flux linkage of the coils during the motion of the suspended mass. Number of turns of each configuration is optimized through load tests on the dynamic workbench. The two moving magnets oscillate around each equilibrium position which are far enough to decouple the electro-mechanical interaction of each mass. m_1 oscillates around the lower part of the tube, inducing a voltage in the lower coils C.1 to C.4, whereas m_2 oscillates around the upper part of the tube and induces a voltage in the upper coils C.7 to C.10 (see Figure 1). Consequently, the optimum coil for each moving magnet can be evaluated considering the decoupled induction effects. These two optimum coils can then be connected in series to couple the induced voltages and maximize the harvester performances. Table 2 reports the optimized electrical variables of the system. All the magnets in the device are made of NdFeB-N42.

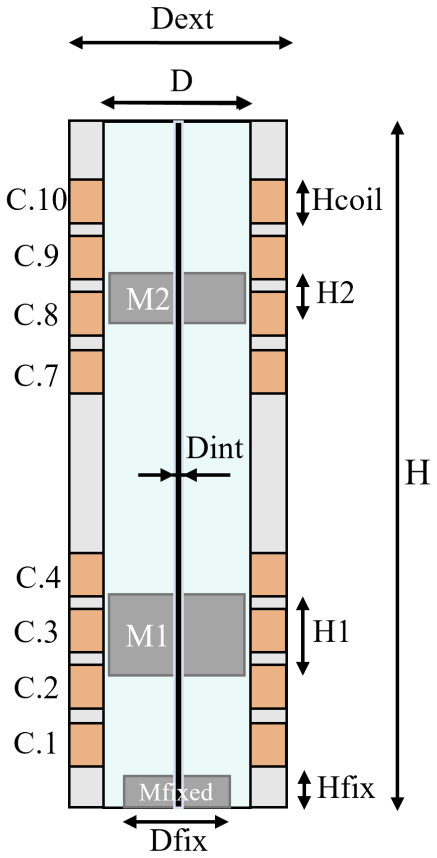

D (mm)	20
Dfix (mm)	10
H1 (mm)	20
H2 (mm)	10
Hfix (mm)	5
Dext (mm)	22
Dint (mm)	4
H (mm)	200
Hcoil (mm)	10
m1 (g)	45
m2 (g)	22.5
Dwire (mm)	0.1
Nturns	500
Rcoil (Ω)	90

Figure 1: Schematic representation of the 2DOF GVEH.

2.2. Linear system analysis

The correct tuning of the two stiffness is crucial in defining the performances of the system. The stiffness of a magnetic suspension depends on the magnetic moments of the two opposing magnets. Consequently, one of the main design variables is the mass ratio of the two moving magnets. A first analysis on a linear 2DOF GVEH model needs to be carried out in order to evaluate the relation between output power, frequency band and the mass ratio. Starting from a 1DOF configuration having optimum design variables (magnets dimensions, tube length, coil position and number of turns, resistive load), different top masses are tested and the corresponding Frequency Response Functions (FRFs) in terms of displacement amplitude and output power are computed for comparison. Figure 2 shows the results of this analysis for mass ratios m_2/m_1 of 0.25, 0.5, 0.75, 1. FRFs are computed solving the linearized version of equations (2)-(3) described in Section 2.3. Changing the mass ratios and the magnetic moments of the moving magnets effects not only the stiffness, but also damping and electromagnetic coupling coefficient values of both DOFs (see Sections 2.3.1-2.3.2). As a result, in the FRFs the resonance frequencies and peak amplitudes change with the mass ratios. As the mass of m_2 increases, also the stiffness k_1 increases even though m_1 mass has a fixed value, shifting the resonance frequenct of DOF 1 to higher values. Stiffness k_2 increases with the mass of m_2 proportionally, leading to an almost constant resonance frequency for DOF 2. As for a dynamic absorber, with increasing value of m_2 mass the displacement amplitude of m_1 decreases. The displacement amplitude of DOF 2 decreases similarly to DOF 1 because higher values of m_2 mass lead to higher electromagnetic damping values. As mass ratios tend to 1, the electromagnetic

coupling coefficient of m_2 grows, leading to an higher output power peak of DOF 2. However, the undesired effect of m_2 is to damp the oscillation of m_1, reducing the output power for resonance of DOF 1. Moreover, with increasing mass ratios, the distance between the two resonance peaks grows far from the frequency value of the 1DOF configuration, resulting in the detuning of the device. The mass ratio of 0.5 shows the best trade-off between overall power enhancement and narrow frequency range between the two resonance peaks. This configuration is used for the complete non-linear analysis described in the following sections. The two eigenfrequencies are evaluated solving the following matrix equation (1) of the linearized free undamped analytical model described in Section 2.2. The linearized stiffness values are evaluated in the equilibrium positions of the two magnets as described in Section 2.3.1.

$$\begin{bmatrix} m_1 & 0 \\ 0 & m_2 \end{bmatrix} \begin{pmatrix} \ddot{x_1} \\ \ddot{x_2} \end{pmatrix} + \begin{bmatrix} k_1 + k_2 & -k_2 \\ -k_1 & k_2 \end{bmatrix} \begin{pmatrix} x_1 \\ x_2 \end{pmatrix} = \begin{pmatrix} 0 \\ 0 \end{pmatrix} \tag{1}$$

Solving the determinant of the equation in the frequency domain allows to evaluate the two eigenfrequencies. Magnetic springs have stiffness values that depend on the magnetic moments and consequently the mass of the moving magnets. Consequently, changing the masses of the moving magnets also changes the linear stiffness values. The eigenfrequencies dependence of both of this variables explains their unusual values during the mass ratio analysis. Table 1 summarizes the eigenfrequencies of the system with the tested mass ratios.

Table 1: Eigenfrequencies of the system with different mass ratios.

Mass ratio m_2/m_1	Eigenfrequency DOF 2 (Hz)	Eigenfrequency DOF 1 (Hz)
0.25	3.30	6.14
0.5	3.33	7.14
0.75	3.28	8.36
1	3.35	9.02

2.3. Analytical model

The analytical model of the generator consists in a 2DOF non-linear mass-spring-damper system. The seismic mass m_1 of the system is a moving magnet suspended thanks to the repulsive force with the fixed magnet at the bottom. The seismic mass m_2 is suspended using the repulsive force with m_1. The stiffness k_1 is related to the first magnetic suspension connecting the fixed magnet and m_1, while k_2 is related to the second one connecting m_1 and m_2, thus depending on their relative motion. The magnetic force between m_2 and the fixed magnet is neglected considering their distance. The damping characteristics derive from two components: mechanical due to viscous action of the air and friction (c_{vis}), electromagnetic due to the induction of parasitic currents in the coils (c_{em}). The mechanical damping (c_{vis2}) is placed between the two masses as its effect depends on their relative motion. Electromagnetic damping (c_{em}) effects depend on the motion of the masses respect to the coils, therefore they are placed between each mass and the fixed base. An external sinusoidal input is applied to the system, generating oscillation motions of the moving magnets. The transducing mechanism consists in the relative motion of the masses inside the tube respect to the coils, creating a time variation of the magnetic flux linkage of the coils and consequently an induced electromotive force. A representation of the system analytical mechanical model is shown in Figure 3a. In order to evaluate the transducing mechanism and the generated power, the electromagnetic subsystem needs to be studied and to be coupled with the mechanical one.

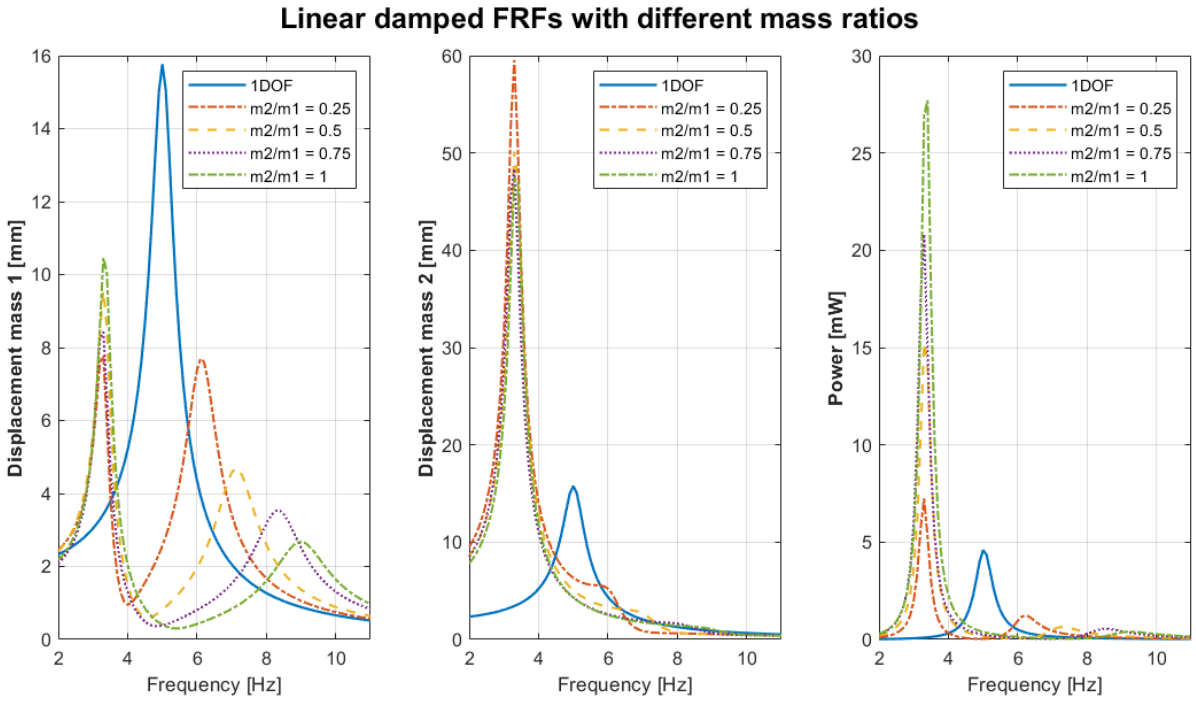

Figure 2: Comparison between FRFs of 1DOF and 2DOF linear damped systems with different mass ratios.

The main electromagnetic characteristics of the harvester are the electromagnetic damping and coupling coefficient. These non-linear physical quantities depend on the time variation of the magnetic flux linkage across the coils. The induced electromotive force and the generated power are directly dependent on the moving magnets speed. The electrical circuit of the system can be described as shown in the Figure 9. The harvester can be considered as an AC generator with its internal resistor R_{coil}, connected to the external resistive load R_{load} that needs to be properly designed through load tests to maximize power. A schematic representation of the electromagnetic circuit of the harvester is reported in Figure 3b. The equation of motion of each degree of freedom (2)-(3) is a time-dependent second order differential equation.

$$m_1\ddot{x_1} + c_{em1}(\dot{x_1} - \dot{y}) + c_{vis1}(\dot{x_1} - \dot{y}) - c_{vis2}(\dot{x_2} - \dot{x_1}) + k_1(x_1 - y) - k_2(x_2 - x_1) = 0 \quad (2)$$

$$m_2\ddot{x_2} + c_{em2}(\dot{x_2} - \dot{y}) + c_{vis2}(\dot{x_2} - \dot{x_1}) + k_2(x_2 - x_1) = 0 \quad (3)$$

Where:

- m_1, m_2 are the seismic mass of the moving magnets
- c_{vis1}, c_{vis2} are the viscous damping of DOF 1 and 2
- c_{em1}, c_{em2} are the electromagnetic damping of DOF 1 and 2
- k_1, k_2 are the non-linear stiffness of the two magnetic springs
- y is the external sinusoidal movement applied to the base, having acceleration amplitude Y_0 and frequency ω

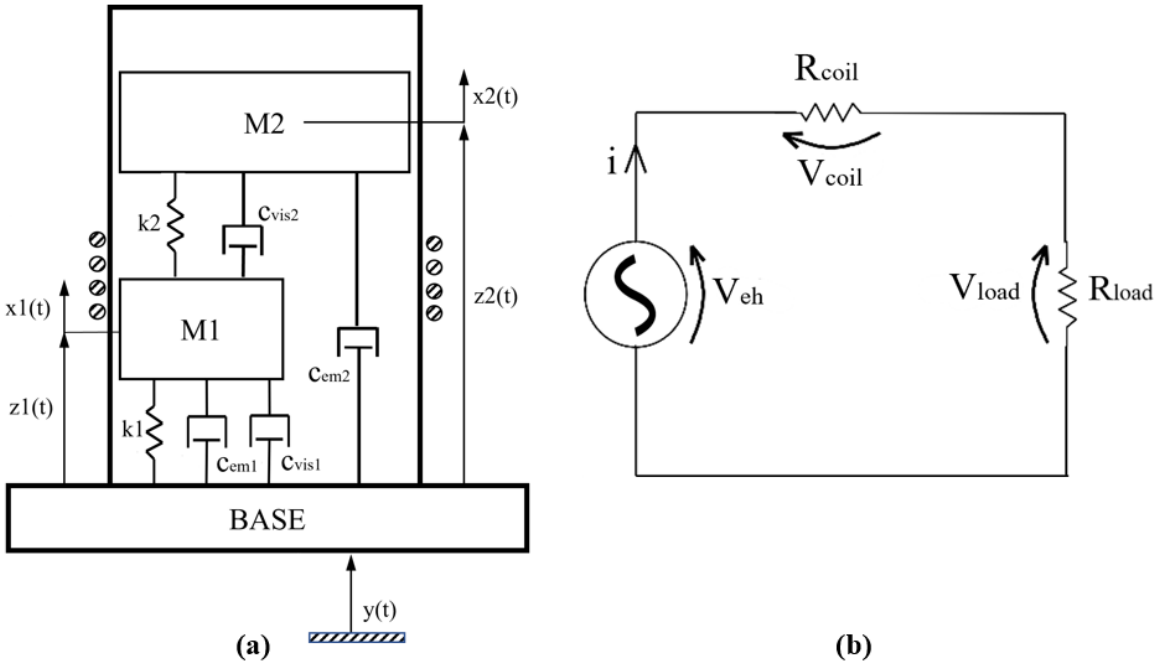

Figure 3: Analytical model of the mechanical (a) and electric (b) subsystem.

Equations (4)-(5) are derived through the implementation of Kirchoff's laws to the circuit of the electromagnetic subsystem.

$$i = \frac{V_{eh}}{R_{coil} + R_{load}} \tag{4}$$

$$P_{load} = V_{load} i \tag{5}$$

The electromagnetic coupling coefficient $k_{em}(z)$ derives from the variation of the magnetic flux during the moving magnet oscillation (6). The coefficient allows to link the voltage to the moving magnet speed (7) and define the electromagnetic damping force acting on the seismic mass (8)-(9).

$$k_{em}(z) = -\frac{d\Phi}{dz} \tag{6}$$

$$V_{eh} = -\frac{d\Phi}{dt} = -\frac{d\Phi}{dz}\frac{dz}{dt} = k_{em}\dot{z}(t) \tag{7}$$

$$F_{em} = k_{em}(z) * i(t) = k_{em}^2(z) * \frac{\dot{z}(t)}{R_{coil} + R_{load}} = c_{em}(z) * \dot{z}(t) \tag{8}$$

$$c_{em}(z) = \frac{k_{em}^2(z)}{R_{coil} + R_{load}} \tag{9}$$

Equations (1)-(8) are implemented in a MATLAB/Simulink model for dynamic simulations of the system to obtain, as solutions, the moving magnets position, speed, acceleration and the induced voltage, current and generated power on the electric load for each time step. The Simulink block scheme is shown in Figure 4. Simulink code is divided into three subsystems, two solving the equations of motion of each degree of freedom and one solving the electromagnetic subsystem. The electromechanical coupling of the three subsystems allows to evaluate the output

electric variables by applying the external mechanical sinusoidal input. Equation (7) describes the computation of the induced electromotive force of each magnet, following the decoupling consideration in Section 2.1. Equation of the two masses are expressed in the variable z, which is the motion coordinate of one of the moving magnet relative to the base motion y with origin in each equilibrium position. The stiffness and damping characteristics need to be defined and inserted in the Simulink model as 1D Look-up Table blocks. Ansys Maxwell software for FEM analyses is essential for this study as it allows to numerically evaluate the characteristics mentioned above. Numerical model of the harvester is built in Ansys Maxwell environment for magnetostatic and transient electromagnetic simulations. Given the axisimmetry of the system a 2D model is sufficient.

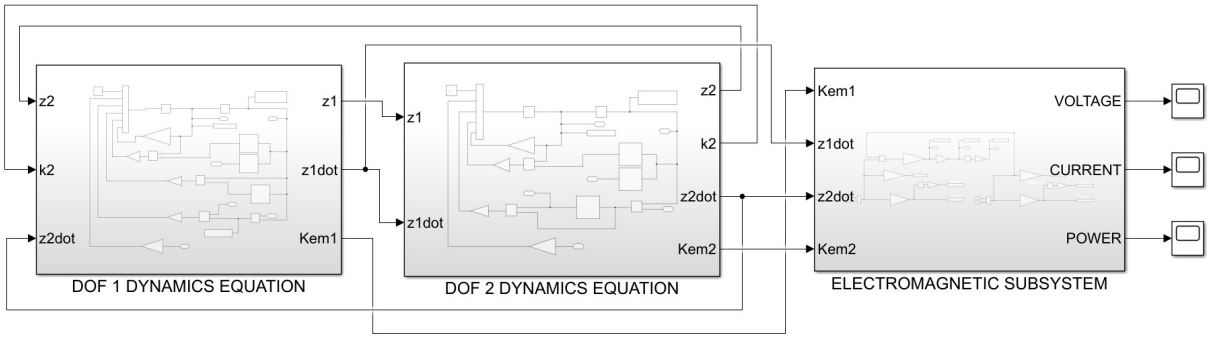

Figure 4: Simulink model.

2.3.1. Mechanical model

The main mechanical characteristics of the harvester are the stiffness of the magnetic springs $k1$, $k2$ and the viscous dampings c_{vis1}, c_{vis2}. Magnetostatic analyses in Ansys Maxwell need to be performed for the definition of the stiffness characteristics. The moving magnets' positions are swept with a fine step along a certain stroke to visualize the distribution of magnetic field vectors, as can be seen in Figure 5.

For every position of the moving magnets, Ansys Maxwell computes the corresponding coenergy $W(x)$ of the system. Coenergy is a physical quantity that is necessary for the evaluation of the harvester stiffnesess. The derivation of the coenergy respect to the suspended mass position results in the magnetic repulsive force acting between two magnets [14] that needs to be interpolated by the best fitting function.

$$F_{mag}(x) = \frac{dW(x)}{dx} \tag{10}$$

As stated in [15], the magnetic force acting between two magnetic dipoles having same magnetic moment and their axes aligned is proportional to $1/x^4$. Even though the three magnets have different magnetic moments, the proposed function fits the simulation data quite precisely. The expression of the function is the following:

$$F_{mag,fit}(x) = \frac{p_1}{x^4 + q_1 x^3 + q_2 x^2 + q_3 x + q_4} \tag{11}$$

The coefficients are determined in MATLAB environment. The stiffness characteristic can be easily obtained by deriving again the magnetic force fitting function respect to x.

$$k(x) = \frac{dF_{mag,fit}(x)}{dx} \tag{12}$$

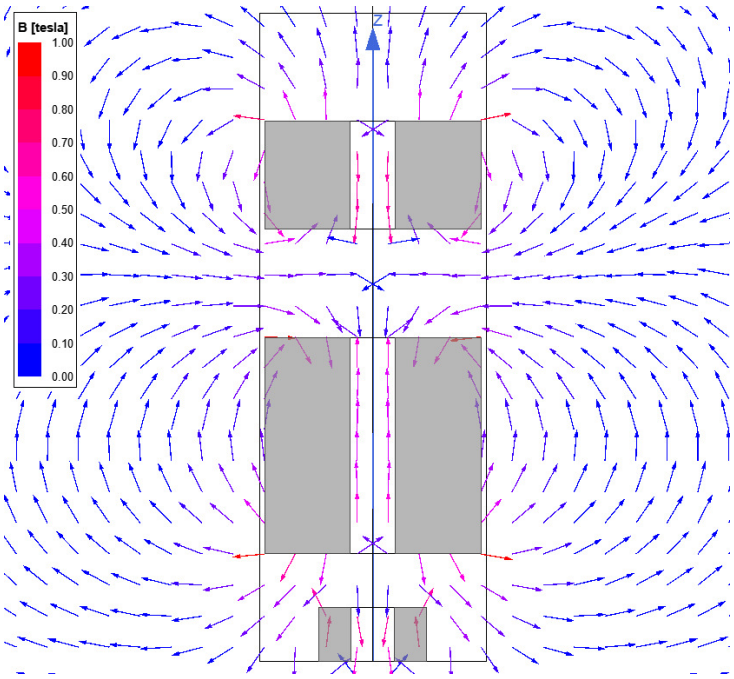

Figure 5: Magnetic field vector of the model.

The two stiffnesses of the magnetic springs are computed one at a time using different approaches. Firstly, stiffness k_2 is evaluated by sweeping m_2 relatively to m_1, starting from its upper face when the two magnets ideally touch and ending to the upper face of the tube. m_1 is positioned at a sufficient distance from the fixed magnet at the base, following the assumption of negligible interaction between m_2 and the fixed magnet. The result is a stiffness characteristic that depends on the relative position between the two moving magnets. Secondly, stiffness k_1 is evaluated by sweeping m_1 from the upper face of the fixed magnet at the base, keeping m_2 fixed in its equilibrium position respect to m_1. Figure 6 shows the plot of the stiffness curves evaluated for m_1 and m_2 in terms of absolute coordinate of the suspended masses x_1 and x_2. In all the following plots of the paper, the displacement value at $x_1 = 0mm$ is ideally considered where $m1$ and fixed magnet are touching, which is also the lower limit of the moving magnet stroke. Whereas, the displacement value at $x_2 = 0mm$ is ideally considered where m_1 and m_2 are touching. The equilibrium positions are evaluated solving the static equations of the two DOFs to obtain the linearized stiffness in the equilibrium positions used in the eigenfrequencies computation in Section 2.2.

The second mechanical characteristic is viscous damping due to air action and surface friction of the moving magnets. It can be considered as a constant and evaluated through experimental tests on the device. Harvester receives a step input and the harvester time response of output voltage signal is processed to extract the damping value. The chosen viscous damping factor equal to 0.04 is the one evaluated by experimental tests on the 1DOF optimized device.

2.3.2. Electromagnetic model

The electromagnetic variables of the circuit introduced in equations (4)-(9) are crucial in determining the output power. Increasing number of turns results in higher coupling coefficient but also greater damping, thus modifying the moving magnet speed and the variation of flux linkage in time.

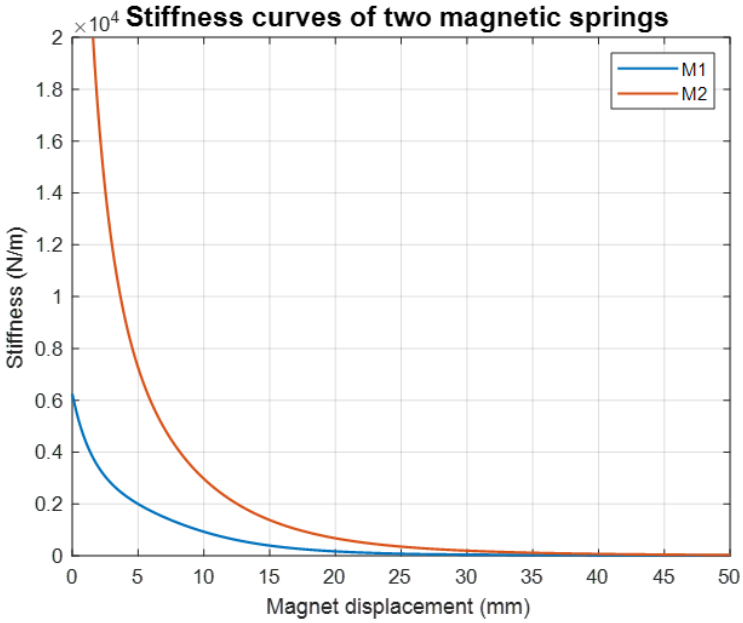

Figure 6: Stiffness curves of the two magnetic springs.

Coils dimensions and location along the tube need to be properly designed in order to extract the maximum amount of power from the system. The coil location along the tube affects the flux linkage variation during oscillation and the dimensions affect the resistance. moreover, optimum value of load resistance needs to be evaluated through load tests for maximum power generation. Transient simulations in Ansys Maxwell enable to evaluate the magnetic flux linkage across the harvester windings. The software allows to plot the magnetic flux lines distribution during the motion of the suspended masses. The plot is reported in Figure 7 with the two moving magnets in the equilibrium position. The plot is useful to visualize where the flux linkage is stronger and how fast it decreases moving away radially from the suspended magnets. As can be noticed, the magnetic flux is maximum around the mass center of the moving magnet. The tube width is a parameter that needs to be designed performing a trade-off between structural rigidity and amount of magnetic flux linkage. The output of the transient analyses is a curve that links the magnetic flux to the absolute displacement of the moving magnet for each coil. Considering that all the coils in each configuration are the same, the curves are identical but shifted along the x-axis due to the different axial locations of the coils. Afterwards, the electromagnetic coupling coefficient and damping curves can be easily determined following equations (5) and (8). These are reported in Figures 8 for two coils and for each moving magnet.

3. Results

The mechanical and electromagnetic characteristics of the harvesters obtained through Ansys Maxwell numerical simulations are used in MATLAB/Simulink environment to perform dynamic simulations of the systems. The most relevant results are the Frequency Response Functions (FRFs) curves that show the resonance peaks and the non-linear behavior of the system. FRFs are computed in terms of load power root mean square values. The sinusoidal excitation input is sweeped in terms of frequency (2-10 Hz) and amplitude (0.2 g-0.5 g). Results are computed using the optimum resistive load $R_{load} = 150\,\Omega$ and connecting one coil at a time in order to evaluate the two optimum coils, one for each moving magnet, that maximize output power.

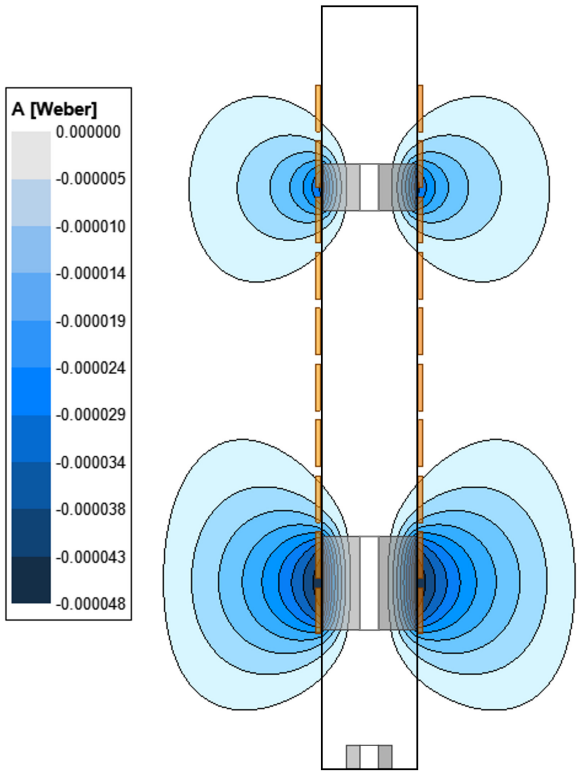

Figure 7: Magnetic flux lines of the model.

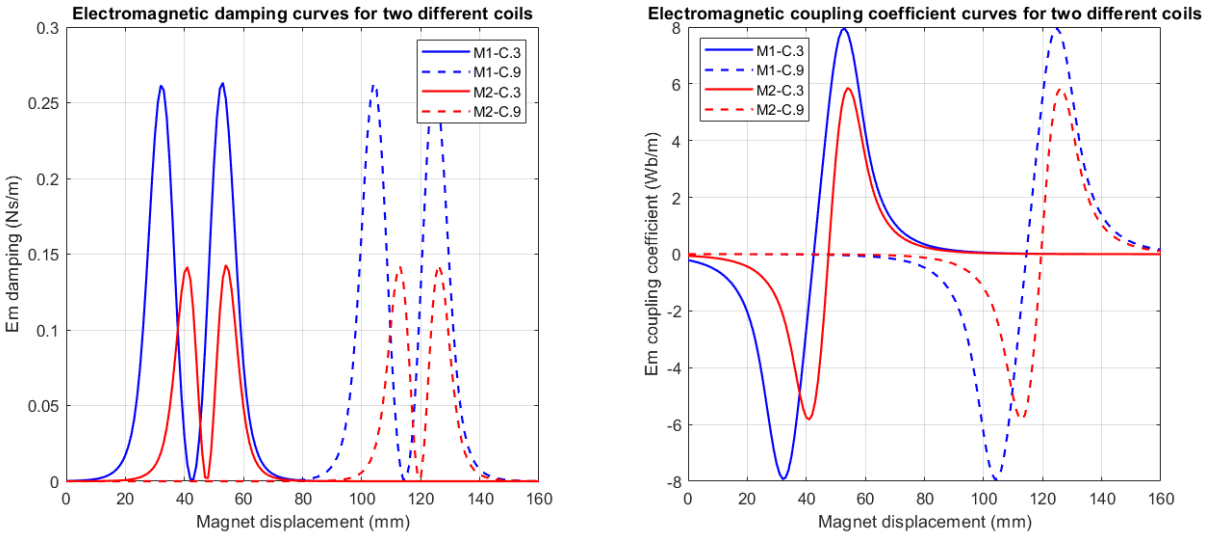

Figure 8: Electromagnetic damping and coupling coefficient curves of the system.

Table 2 shows the power resonance peaks for external excitation amplitude of 0.5 g and connecting one coil at a time. C.3 and C.9 are the optimum coils that maximize the power respectively for m_1 and m_2. Figure 9a-9b show the complete computation of the FRFs for C.3 and C.9 with excitation amplitudes from 0.2 g to 0.5 g in the frequency range of 2-10 Hz. FRF for C.3 has the highest power peaks but has low efficiency in the frequency range of 4-6 Hz.

Table 2: Power resonance peaks for different coils and external excitation amplitude of 0.5 g.

Coil number	Resonance peak 1 (mW)	Resonance peak 2 (mW)
C.1	9.42	4.79
C.2	11.67	6.74
C.3	16.28	6.87
C.4	15.57	6.30
C.7	5.52	2.00
C.8	10.26	3.34
C.9	11.9	3.68
C.10	11.58	3.58

FRF for C.9 has still high power peak and shows a wider frequency band, up to 6 Hz, where the output generation is considerable. Following the consideration in Section 2.1 of decoupled electromotive force induction of the two magnets, the series connection of C.3 and C.9 should give as output an intermediate solution that combines the benefits of the single coils. Figure 10b reports the complete FRFs for the series connection of C.3 and C.9, while Figure 10a shows the comparison between FRFs of the series connection and the single coils for 0.4 g excitation amplitude. As can be clearly noticed, the series connection shows the best results in terms of power generation and frequency broadband, thus maximizing the efficiency of the device.

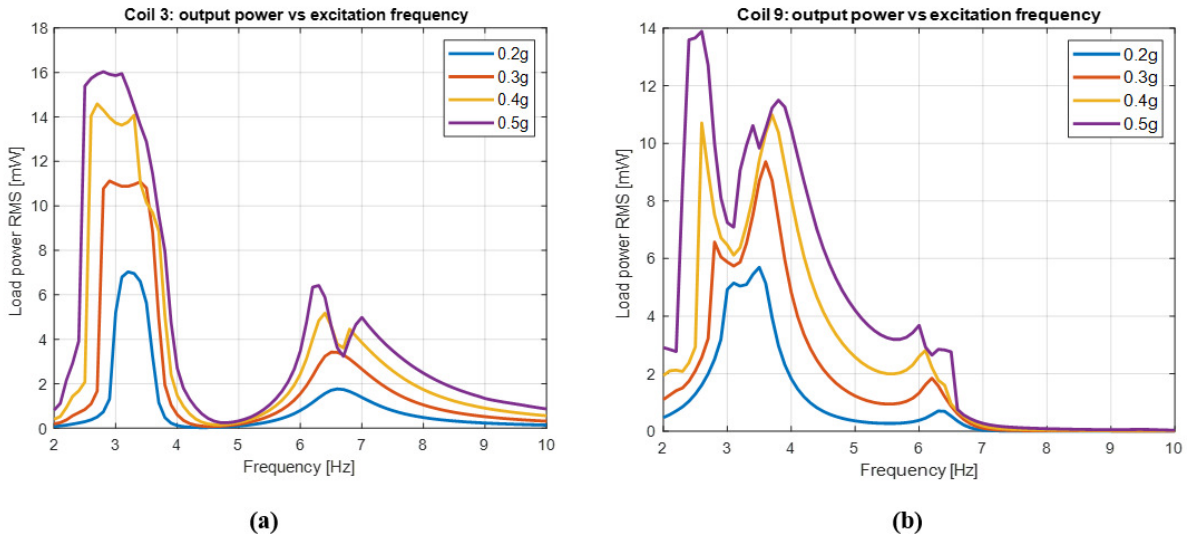

Figure 9: FRFs for C.3 (a) and C.9 (b).

4. Discussions

FRFs plots convey crucial information about generated power intensity and resonance frequencies. As can be seen in Figures 9-10, the resonance peak of DOF 1 around 6 Hz is lower than the peak of DOF 2 around 3 Hz. This behavior is connected to the damping effect that m_2 has on the vibration amplitude of m_1 due to the dynamic absorber configuration. Equation (6) shows that the induced voltage is the result of the product between the electromagnetic coupling coefficient and the magnet speed.

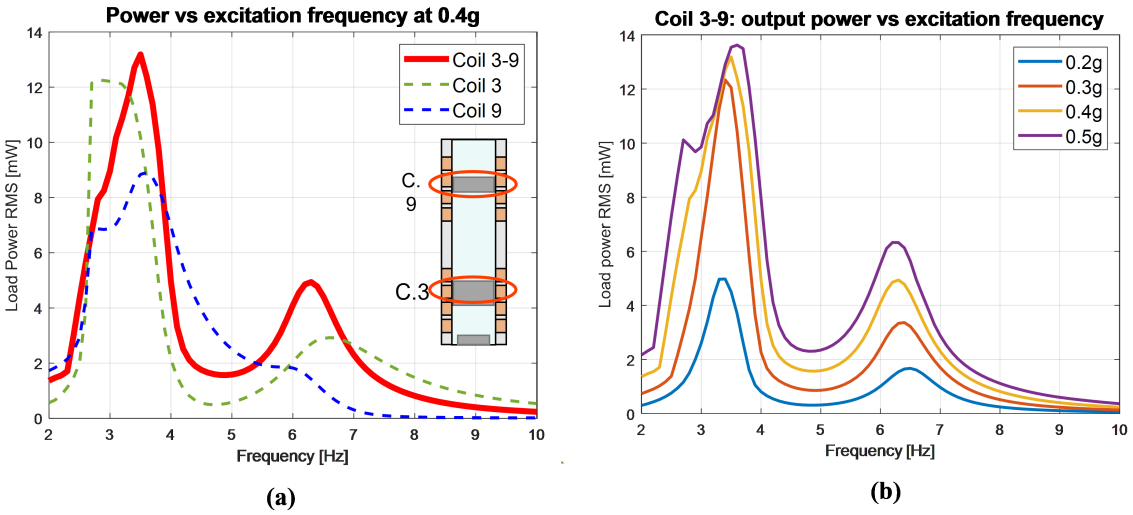

Figure 10: Comparison between FRFs with series connection and single coils (a) FRFs for series connection C.3 and C.9 (b).

Even though m_1 has a bigger magnetic moment and consequently higher coupling coefficient than m_2, the damping effect on the speed prevails. In order to have a deeper insight and better visualization of the system dynamics, a Simpack model is built for Multibody simulations and compared to the Simulink results. Resonance peak of DOF 1 has an eigenmode of vibration with anti phase motion of the two masses, while eigenmode of DOF 2 is in phase. As can be noticed in Figures 11-12, antiphase condition has lower vibration amplitudes than the in phase one, leading to the lower power peak of DOF 2. Moreover, FRFs can be analyzed to understand and quantify the benefits of a 2DOF system compared to a 1DOF one. The area under the curve for RMS power FRFs can be used as a term of comparison between the two configurations, as it considers both the peak amplitudes and the frequency band. Figure 13 reports this analysis, considering the RMS power of 2 mW as the low threshold of useful output power quantity. 2DOF system carries an increase in terms of power area of 24% and in terms of useful frequency band of 13% respect to 1DOF configuration, thus validating the efficiency benefits of a 2DOF configuration.

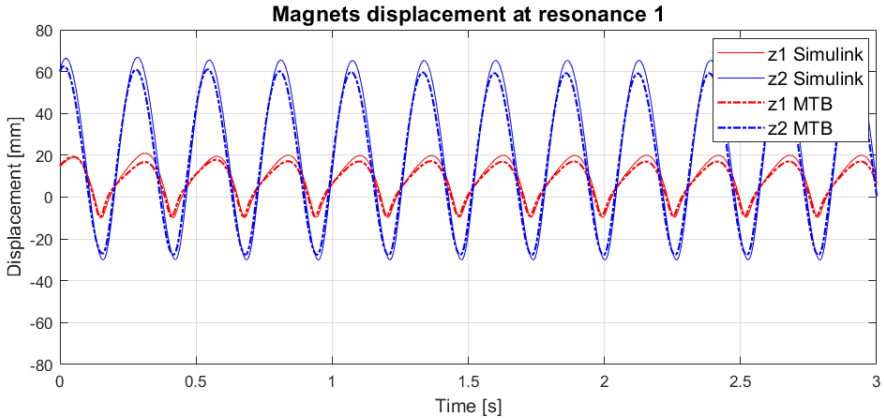

Figure 11: Multibody and Simulink simulations of in phase magnets displacement at resonance of DOF 1.

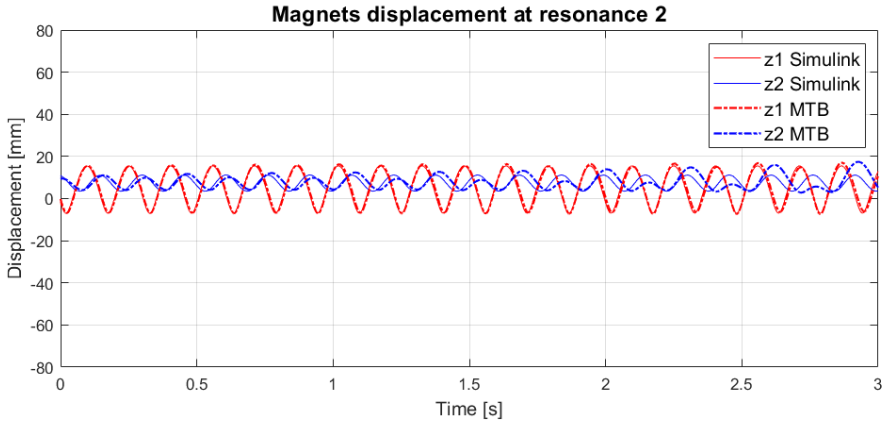

Figure 12: Multibody and Simulink simulations of antiphase magnets displacement at resonance of DOF 2.

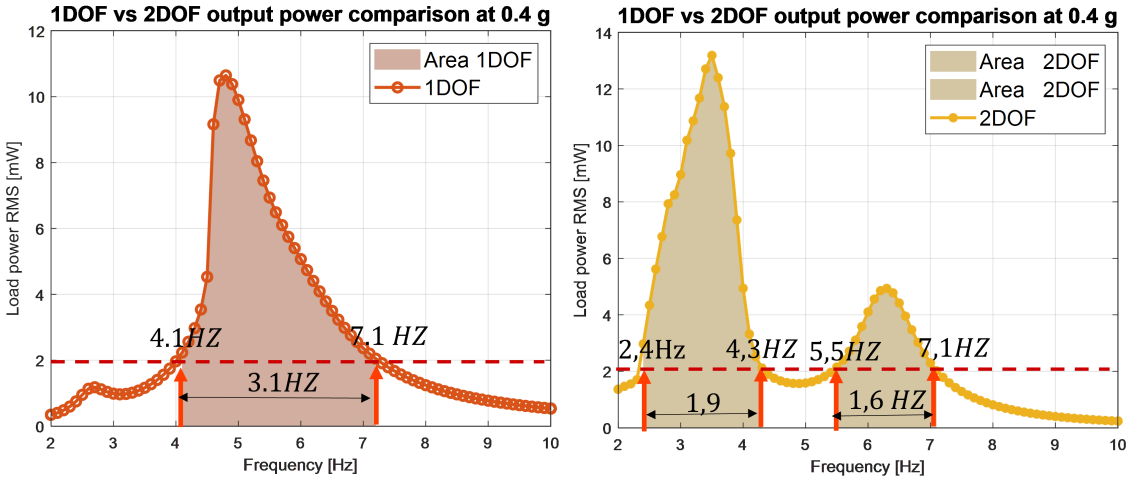

Figure 13: Area under the curve comparison of 1DOF-2DOF areas under the curve of RMS power FRFs.

$$Area\ efficiency\ index\ (\%) = \frac{Area_{2DOF} - Area_{1DOF}}{Area_{1DOF}} * 100 \tag{13}$$

$$Bandwidth\ efficiency\ index\ (\%) = \frac{Bandwidth_{2DOF} - Bandwidth_{1DOF}}{Bandwidth_{1DOF}} * 100 \tag{14}$$

4.1. Conclusions

This work presents the design methodologies of a 2DOF vibrational energy harvester. A preliminary study of this device was carried out to evaluate the power and the frequency bandwidth enhancements compared to a 1DOF device. A model in Simulink/Matlab was realized starting from the coupled mechanical dynamic equations and electromagnetic ones. For the computation of the magnetic suspension stiffness characteristic and the time-variation of the flux linkage, a model on ANSYS Maxwell was developed for FEM simulations. Moreover, Multibody simulation were executed to support the authors in the prototyping phase for further understanding of the system dynamics. The results of these simulations are promising and solid.

An increase of 26 % in terms of the area under the curve of RMS power above a 2 mW threshold was obtained, along with an increase of 16 % in high-power frequency bandwidth. These first results demonstrate how a 2DOF device can be beneficial in terms of efficiency for the supply of IoT devices, compared to a 1DOF system. The next steps of this work will regard the realization of a modular prototype in order to perform the required experimental tests to validate the model proposed in this paper.

References

[1] Dewan A, Ay S U, Karim M N and Beyenal H 2014 Alternative power sources for remote sensors: A review
[2] Singh J, Kaur R and Singh D 2021 Energy harvesting in wireless sensor networks: A taxonomic survey
[3] Majid M, Habib S, Javed A R, Rizwan M, Srivastava G, Gadekallu T R and Lin J C W 2022 *Sensors* **22**(6) ISSN 14248220
[4] Pasquale G D, Somà A and Zampieri N 2012 *Journal of Computational and Nonlinear Dynamics* **7**(4) ISSN 15551423
[5] Russo C, Monaco M L, Fraccarollo F and Somà A 2021 *Energies* **14**(15) 4622 ISSN 1996-1073
[6] Russo C, Monaco M L and Somà A 2022 *IOP Conference Series: Materials Science and Engineering* **1214**(1) 012046 ISSN 1757-8981
[7] O'Donoghue D, Frizzell R, Kelly G, Nolan K and Punch J 2016 *Smart Materials and Structures* **25**(5) ISSN 1361665X
[8] Rodriguez J C, Nico V and Punch J 2019 *Sensors (Switzerland)* **19**(17) ISSN 14248220
[9] Fan K, Zhang Y, Liu H, Cai M and Tan Q 2019 *Renewable Energy* **138** 292–302 ISSN 18790682
[10] Ung C, Moss S D and Chiu W K 2015 vol 9431 (SPIE) p 94312C ISBN 9781628415346 ISSN 1996756X
[11] Feng Z, Peng H and Chen Y 2021 *Energies* **14**(22) ISSN 19961073
[12] Carneiro P, dos Santos M P S, Rodrigues A, Ferreira J A, Simões J A, Marques A T and Kholkin A L 2020 *Applied Energy* **260** 114191 ISSN 03062619
[13] Santos M P S D, Ferreira J A, Simões J A, Pascoal R, Torrão J, Xue X and Furlani E P 2016 *Scientific Reports* **6** ISSN 20452322
[14] Fu W, Zhou P, Lin D, Stanton S and Cendes Z 2004 *IEEE Transactions on Magnetics* **40**(2) 683–686 ISSN 0018-9464
[15] Kraftmakher Y 2007 *European Journal of Physics* **28**(3) 409–414 ISSN 0143-0807